



The German Aerospace Center M-42 radiation detector—A new development for applications in mixed radiation fields

Cite as: Rev. Sci. Instrum. **90**, 125115 (2019); <https://doi.org/10.1063/1.5122301>

Submitted: 30 July 2019 . Accepted: 02 December 2019 . Published Online: 19 December 2019

T. Berger , K. Marsalek , J. Aeckerlein, J. Hauslage , D. Matthia , B. Przybyla , M. Rohde, and M. Wirtz



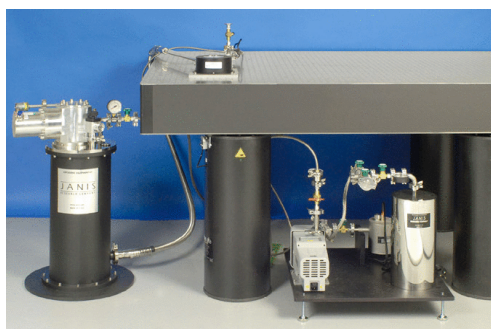
View Online



Export Citation



CrossMark



JANIS

Rising LHe costs? Janis has a solution.
Janis' Recirculating Cryocooler eliminates the use of Liquid Helium for "wet" cryogenic systems.

sales@janis.com www.janis.com [Click for more information.](#)

The German Aerospace Center M-42 radiation detector—A new development for applications in mixed radiation fields

Cite as: Rev. Sci. Instrum. 90, 125115 (2019); doi: 10.1063/1.5122301

Submitted: 30 July 2019 • Accepted: 2 December 2019 •

Published Online: 19 December 2019



T. Berger,^{a)} K. Marsalek, J. Aeckerlein, J. Hauslage, D. Matthiä, B. Przybyla, M. Rohde, and M. Wirtz

AFFILIATIONS

German Aerospace Center (DLR), Institute of Aerospace Medicine, Linder Hoehe, 51147 Cologne, Germany

Note: This paper is part of the Special Collection: Materials and Life Science Experiments for the Sounding Rocket MAPHEUS.

^{a)}Author to whom correspondence should be addressed: thomas.berger@dlr.de

ABSTRACT

In the last few years, the Biophysics Working Group of the Institute of Aerospace Medicine of the German Aerospace Center (DLR) started the development of a small low power consumption radiation detector system for the measurement of the absorbed dose to be applied in various environments, such as onboard aircraft, in space, and also as a demonstration tool for students. These so called DLR M-42 detectors are based on an electronics design, which can easily be adjusted to the user- and mission-requirements. M-42 systems were already applied for measurements in airplanes, during two MAPHEUS (Materialphysikalische Experimente unter Schwerelosigkeit) rocket missions, and are currently prepared for long term balloon experiments. In addition, they will be part of the dosimetry suite of the upcoming Matroshka AstroRad Radiation Experiment on the NASA Artemis I mission. This paper gives an overview of the design and the testing of the DLR M-42 systems and provides highlighted results from the MAPHEUS campaigns where the detectors were tested for the first time under space flight conditions. Results clearly show that the system design enables independent measurements starting upon rocket launch due to the built-in accelerometer sensors and provides data for the relevant 6 min of μ -gravity as given for the MAPHEUS missions. These 6 min of the μ -gravity environment at altitudes between 100 and 240 km lead to a total absorbed dose of $1.21 \pm 0.15 \mu\text{Gy}$ being equivalent to half a day of radiation background measured with the M-42 in the laboratory at DLR, Cologne, Germany.

© 2019 Author(s). All article content, except where otherwise noted, is licensed under a Creative Commons Attribution (CC BY) license (<http://creativecommons.org/licenses/by/4.0/>). <https://doi.org/10.1063/1.5122301>

I. INTRODUCTION

The radiation environment in space, the related exposure to humans, and the possible risk of increased cancer probability are seen as one of the major obstacles to overcome for long duration human space missions beyond Low Earth Orbit (LEO). The measurement of the radiation environment hereby provides one tool for the assessment of the radiation exposure in addition to the possibility to calculate the exposure applying various tools such as Monte Carlo transport codes or deterministic transport codes. Radiation detectors have been applied for this aim since the beginning of the space age.¹ They can be based on either passive radiation detector systems such as thermoluminescence detectors and nuclear track etch detectors² or active, powered devices (see review in Ref. 3).

For active devices, detectors based on silicon detector technology are currently the main systems used for space application purposes.

These detectors are either applied as single silicon detector systems [Liulin,^{4,5} RADOM (RADiation DOse Monitor),⁶ and DB-8^{7,8}], put together as silicon detector telescopes [DOSTEL (DOSimetry TELscope)⁹ and TriTel (Three-Dimensional Silicon detector telescope)¹⁰], use silicon strip detectors arranged in x/y/z combination [ALTEA (Anomalous Long Term Effects on Astronauts)¹¹] or use a combination of silicon detectors and organic scintillators [MSL-RAD (Mars Science Laboratory-Radiation Assessment Detector)¹²⁻¹⁴ and ISS-RAD (International Space Station-Radiation Assessment Detector)¹⁵] for the determination of the radiation field parameters. In recent years, new technologies such as the Timepix detector systems evolved, which will be used in the operational

detector system called HERA¹⁶ (Hybrid Electronic Radiation Assessor) for the NASA Artemis missions.

The Biophysics group at DLR started the development of silicon radiation detector systems in recent years and launched in December 2018 the silicon detector telescope RAMIS (Radiation Measurements In Space), which is currently flying onboard the DLR Eu:CROPIS (Euglena gracilis: Combined Regenerative Organic-food Production In Space) mission measuring the radiation environment at approximately 600 km altitude in a polar orbit.¹⁷

In addition to the RAMIS system, the group has worked on a family of miniaturized radiation detector instruments, the DLR M-42 systems. These instruments were developed based on the following internal DLR requirements: they should be small, lightweight, have very low power consumption, have various built-in environmental sensors, such as temperature, pressure, and acceleration, and should be able to be adjustable for the energy deposition range within the radiation detector. At the end, the system shall be easily adaptable for relevant research purposes and should be and will be used as “plug and play” instruments for radiation protection dosimetry. It is currently foreseen to use M-42 detectors as part of NASA scientific balloon campaigns in the USA and over Antarctica as well as applying the systems as one part of the radiation detector suite for the upcoming NASA Artemis I mission to the Moon in the frame of the Matroshka AstroRad Radiation Experiment (MARE).

II. THE DLR M-42 RADIATION DETECTOR

Section II will provide an overview of the DLR M-42 detector family currently used within the department and describe the

relevant features of the systems in terms of electronics and mechanical design.

A. M-42: Block diagram

The overall block diagram for the M-42 electronics design is provided in Fig. 1. The radiation detector applied within the M-42 instruments is a planar silicon PIN photodiode of the type Hamamatsu S3590-19 with an active area of $11.0 \times 11.2 \text{ mm}^2 = 1.23 \text{ cm}^2$ and a thickness of $300 \mu\text{m}$. The bias voltage of 53 V ensures that the detector is fully depleted. The bias voltage is provided by the power generation and conditioning board. When a particle deposits energy in the detector, the released electron charge is amplified in the preamplifier section of the analog electronics. The respective output signal is fed to a shaping circuitry and consecutively to the peak detector. The voltage of each peak is A/D converted (65 536 channels) and passed on to the μ -controller as a digital value. The pulse-height spectral data are stored concurrently into two nonvolatile data flash memory chips. The microcontroller controls a micro-universal serial bus (USB) data interface and the power generating and conditioning unit.

The M-42 family is built-in a modular way in terms of provision of power to the system. On one hand, all instruments can be powered over the micro-USB connector. On the other hand—depending on the M-42 system—power can be provided over either primary Li batteries or rechargeable Li-ion batteries.

B. M-42 versions

Up to now three different versions of the M-42 dosimeter system have been developed at DLR. These versions are the

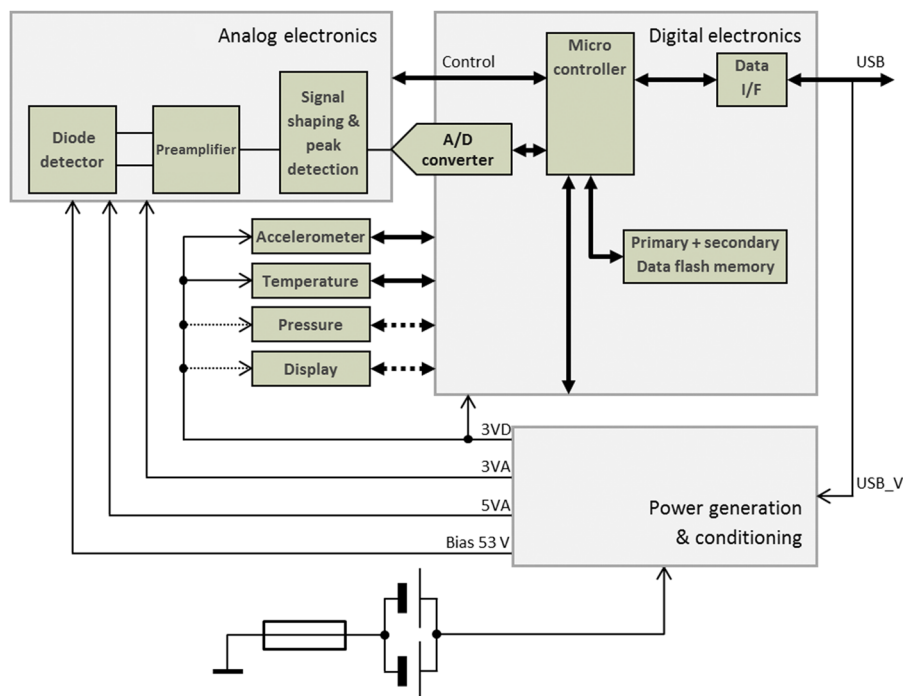


FIG. 1. The DLR M-42 block diagram.

TABLE I. M-42 system overview.

	M-42_C	M-42_S	M-42_D
Dimensions (mm ³)	142 × 38 × 13	54 × 38 × 13 106 × 38 × 13	182 × 44 × 22
Mass w/o batteries (g)	108	120	...
Mass w. batteries (g)	144	156	237
Energy min. (MeV) Si	0.06	0.06	0.06
Energy max. (MeV) Si	18	18	43
Power			
	Micro-USB	X	X
	Primary batteries	X	...
	Rechargeable batteries	...	X
Display + push-button	X
Accelerometer sensor	X	X	X
Temperature sensor	X	X	X
Pressure sensor	X

M-42 Compact (M-42_C), the M-42 Split (M-42_S), and the M-42 Display (M-42_D). Table I provides an overview of the three versions of the M-42 detector system with mass, dimensions, relevant in built environmental sensors, as well as energy resolution of the applied silicon detectors.

Figure 2 provides a picture of the baseline M-42_C system from which all further developments of the detectors have been derived. Figure 2(a) shows the mechanical envelope of the M-42_C, while Fig. 2(b) gives the view of the electronic board with the analog section including the silicon detector diode and the digital part including the two connectors for primary Li batteries and the micro-USB connector.

Figure 3 shows the envelope for the M-42_S detector system. For this system, the design goal was to separate the detector head from the readout electronics, thereby using the head for measurements in confined spaces, and specifically to include it within anthropomorphic phantoms to enable dosimetry measurements at various organ positions inside these phantoms, as was previously done by different detector systems (SSDs) in the frame of the ESA Matroshka experiment¹⁸ and for ground based applications.¹⁹

Figure 4 provides the envelope for the M-42_D system, which is additionally equipped with a small display enabling real time data view of the count and dose rate measured as well as indication of the total dose for a certain time frame.

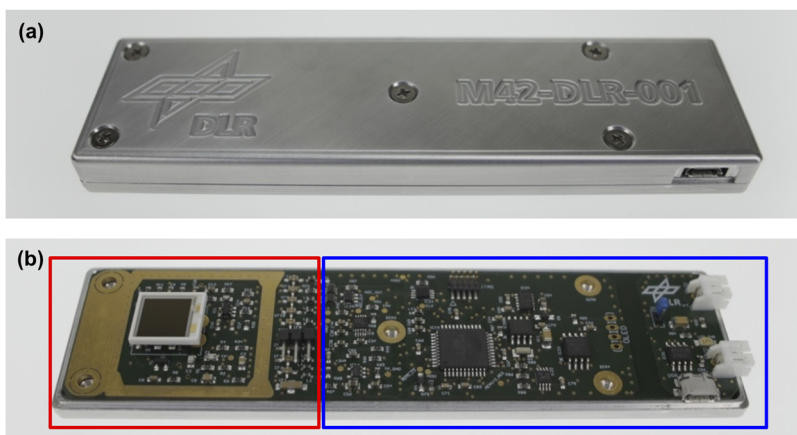


FIG. 2. The DLR M-42_C: (a) M-42_C closed and (b) M-42_C open with the analog part of the system with the silicon detector in red and the digital part of the system with two battery connectors and the micro-USB connector in blue (size: 142 × 38 × 13 mm³).



FIG. 3. The DLR M-42_S (size: 54 × 38 × 13 mm³ for the detector head and 106 × 38 × 13 mm³ for the digital electronics).



FIG. 4. The DLR M-42_D with display (size: 182 × 44 × 22 mm³).

C. M-42 power

All M-42 systems can be powered over the nominal micro-USB interface. In addition, the M-42_C and M-42_S detectors are nominally powered over two primary Li batteries with a capacity of 2600 mAh each. In this configuration, the measurement time of the device is up to 76 days (see also Subsection III B). The M-42_D is nominally powered over two rechargeable Li-ion batteries with a capacity of 1260 mAh each. Charging of these batteries is done over the micro-USB port. In this configuration, the measurement time of the device is six weeks.

D. M-42 accelerometer and modes of operation

To cope with various mission scenarios for space missions, the M-42 family is equipped with a built-in accelerometer sensor. This allows the system to be in standby mode (SLEEP MODE) for an extended period with very low power consumption and to be switched into measurement mode (MEAS MODE) only upon launch of a spacecraft which increases the possible duration of the measurement significantly. Prior to the lift-off the device resides in SLEEP MODE with reduced power consumption. The lift-off is automatically detected by using the built-in accelerometer. The detection algorithm can exclude false positive incidents caused by mechanical shocks that last for a shorter period of time (<5 s). After the lift-off is detected, the device enters the MEAS MODE and this mode status is stored into the nonvolatile memory. If for any reason the μ -controller is being reset (watchdog), after the reboot the device continues data acquisition in the measurement mode. The main reason to have the possibility of the SLEEP MODE is the reduced current consumption. While the nominal MEAS MODE has a current consumption of 2.9 mA, this is reduced in SLEEP MODE to 0.7 mA.

E. M-42 data

The measurement data are stored redundantly on two non-volatile data flash memories. The measured data consist of the internal housekeeping (H/K) data that includes data from the internal temperature (all systems) and pressure (M-42_D) sensors as well as internal supply voltages. H/K data are used to check the sanity of the system.

The main data are of course the science data from the radiation detectors. M-42 records energy depositions from 0.06 MeV to 18 MeV (M-42_C and M-42_S) and up to 43 MeV (M-42_D) in Si. The deposited energy of each detected particle is A/D converted to 65 536 channels, giving the raw Analog to Digital Converter (ADC) resolution of 0.305 keV. To account for the exponential nature of the spectrum, the energy is resampled to logarithmically equidistant

energy intervals (bins). M-42 resolves 224 energy bins. The initial energy resolution at 0.06 MeV is 1.5 keV (M-42_C/M-42_S) and 1.8 keV (M-42_D), and the final resolution at 18 MeV yields 0.5 MeV (M-42_C/M-42_S) and at 43 MeV (M-42_D) around 1.25 MeV. Energy deposition spectra are stored every 5 minutes. Based on the energy deposition in the respective channels, the absorbed dose (D) in Si (unit 1 Gy = 1 J/kg) is calculated by summing up the energy depositions and dividing them by the mass of the detector. Since for radiation protection purposes, the absorbed dose is given either in tissue or water, a conversion factor of 1.23 is applied for the conversion from D in Si to D in H₂O.²⁰ Count- and dose rate data are stored every minute. Both time intervals are user-configurable.

F. M-42 display

In addition to the basic design of the M-42, the M-42_D version has a display and a push-button, which enables the user to operate the device. The current time, the dose rate, and the accumulated dose since the last reset are displayed (see Fig. 5). Thus, the user can monitor the radiation measurements in real time. The display is equipped with backlight to ensure the readability even in a dimly lit environment. If the push-button is pressed, the backlight is switched on immediately and different actions can be triggered depending on the time, for how long the button was pressed (Table II). If the device is set to standby mode, functionalities to wake up the device are

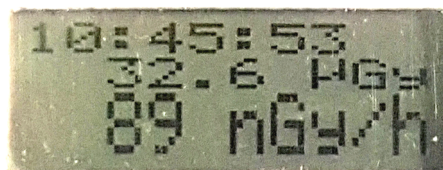


FIG. 5. The display of the DLR M-42_D showing system time (UTC), total dose accumulated since measurement started (32.6 μ Gy in 16.75 days), and the current dose rate (89 nGy/h).

TABLE II. Possible actions triggered by the push-button.

Time	Action	Releasing button
$t < 5$ s	Normal operation	No special effect
5 s $\leq t < 10$ s	Dose is blinking	Set dose to zero
10 s $\leq t < 15$ s	Whole display is blinking	Device enters power down mode
$t > 15$ s	Normal operation	No special effect

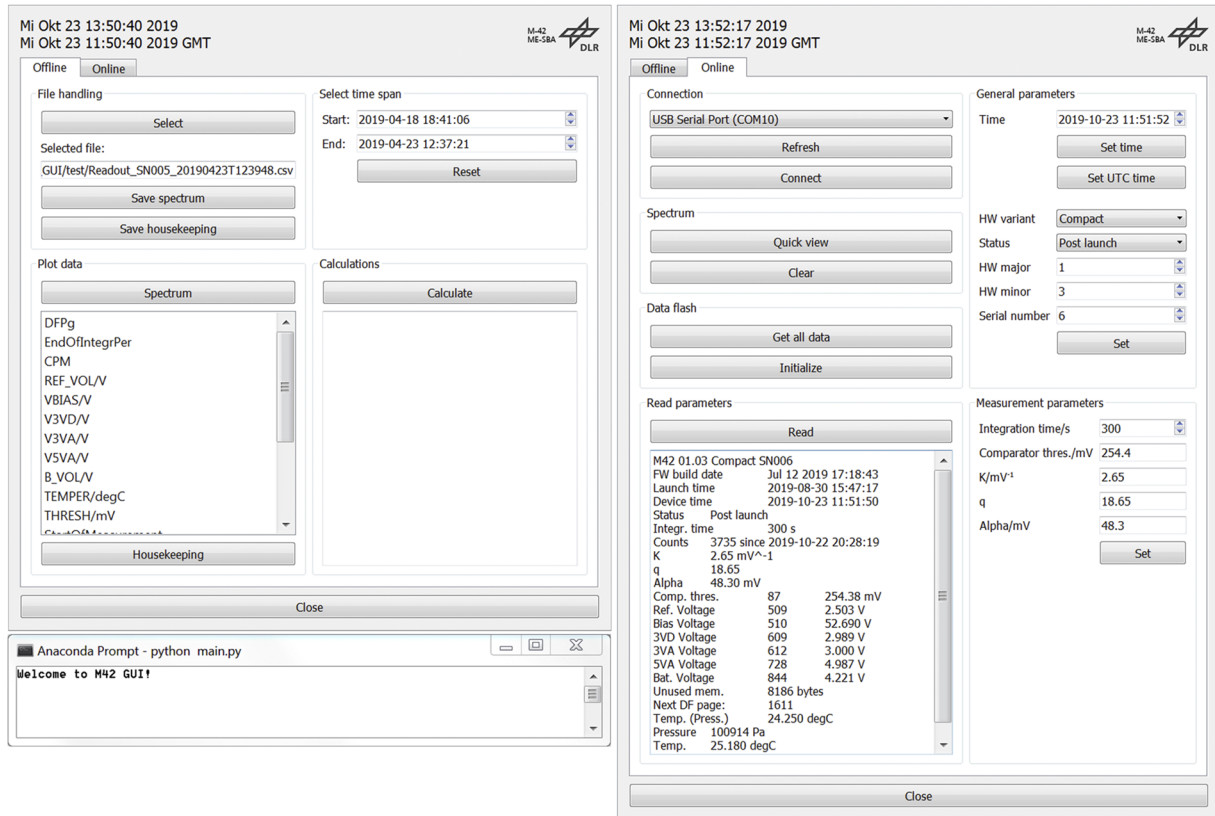


FIG. 6. M-42 GUI (left: offline-processing and right: online-processing).

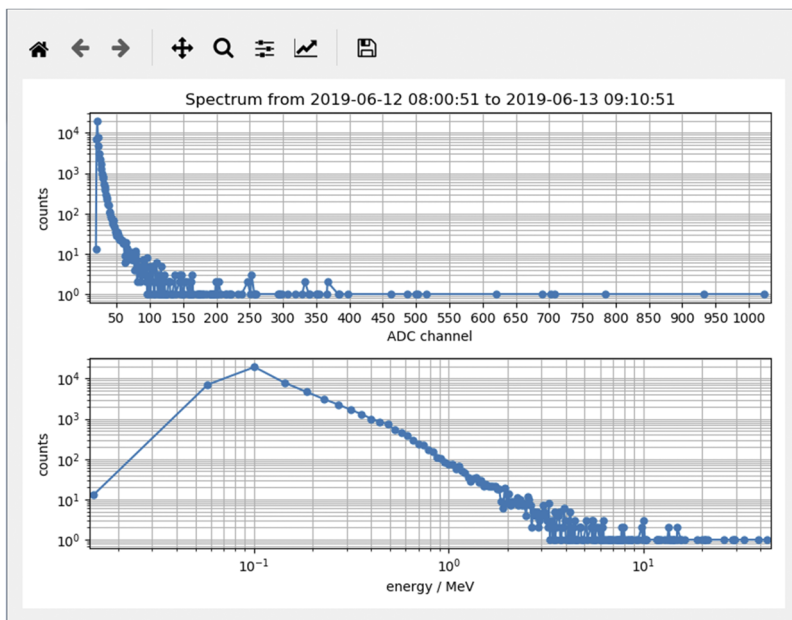


FIG. 7. M-42 GUI real time data. Upper panel: counts vs ADC channel and lower panel: counts vs energy deposition in Si for radiation background measurements at DLR.

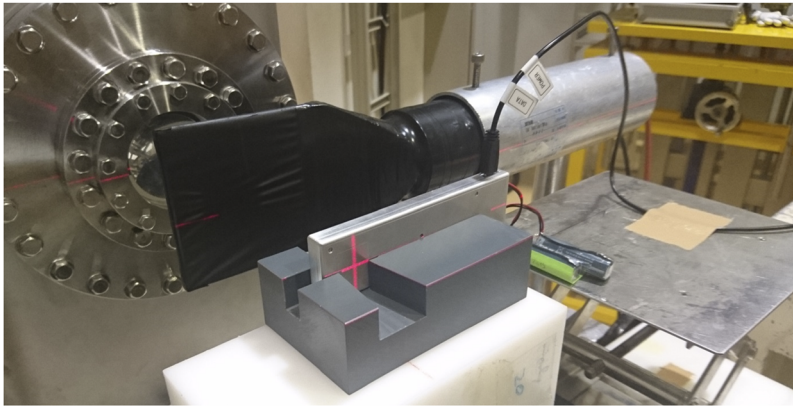


FIG. 8. The setup of the M-42_C detector for energy calibration and testing at the Physics Room of the HIMAC, NIRS, Japan. The red cross indicates the silicon detector position within the M-42_C system adjusted to the beam location.

powered. Unnecessary parts are turned off. To wake up the device, the button must be pressed again.

G. M-42 graphical user interface

The M-42 graphical user interface (GUI) consists of the input mask itself and a terminal window. The terminal window is also used to display information about the previous performed actions and detailed error messages (Fig. 6).

Important messages are also displayed in pop-up message boxes. Due to this separation, the user is not interrupted by unnecessary detailed messages. The input mask in combination with the terminal window is shown in Fig. 6. The size of the widgets is adapted depending on the size of the whole mask automatically. On top, the current local time and the Universal Time Coordinated (UTC)

time are displayed. The tabs below are used to take into account the online- and offline-processing. At the bottom, a button to close the whole application is included. The developed GUI supports two ways off interactions: (a) processing of data that have been already read out and stored on the computer (Fig. 6, offline-processing) and (b) commanding the M-42 device itself (Fig. 6, online-processing). The GUI has the capability to visualize the recorded and live data, e.g., using plots. An example of such a plot is depicted in Fig. 7, where an energy deposition spectrum for background radiation measurements performed at DLR is shown.

III. M-42 TESTS

Section III will describe various tests for the M-42 dosimeter family to (a) determine the functionality of the system itself

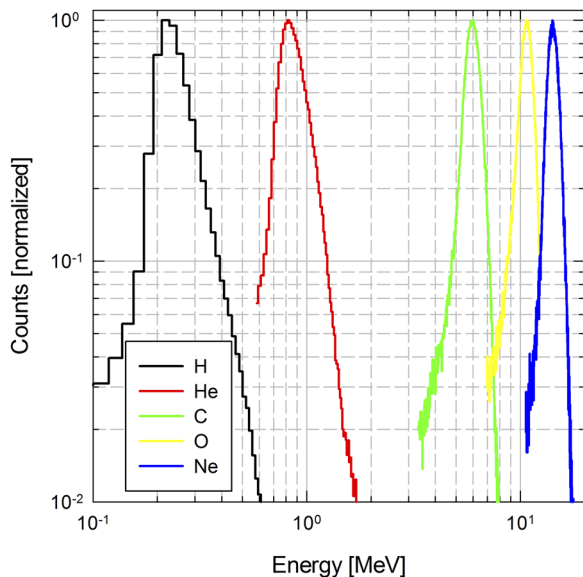


FIG. 9. Energy deposition spectra measured with the M-42_C instrument at NIRS, HIMAC, Chiba, Japan, for protons (180 MeV), helium (230 MeV/n), carbon (400 MeV/n), oxygen (400 MeV/n), and neon (600 MeV/n) ions.

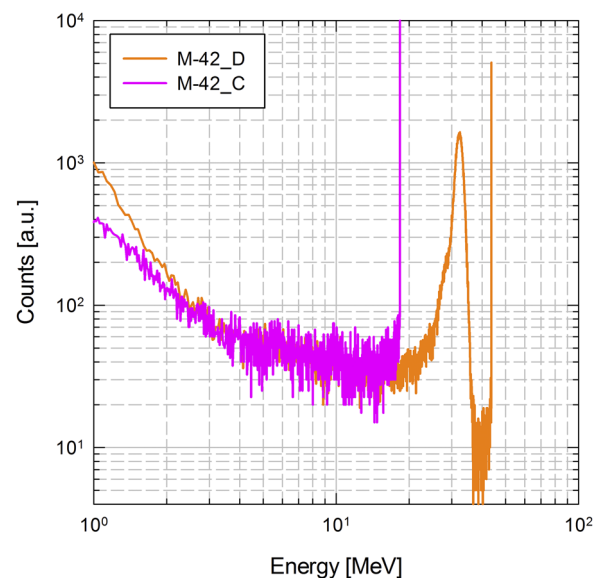


FIG. 10. Energy deposition spectra measured with the M-42_C (pink) and the M-42_D (orange) instrument for silicon ions with a primary energy of 490 MeV/n.

and (b) ensure the proper function in relevant radiation calibration fields.

A. Energy calibrations at NIRS, HIMAC, Japan

The nominal linearity of the electronics chain of the system was determined by using test pulses, thereby providing the overall dynamic range of the system. Internally, at DLR further energy calibrations were performed by placing the detector inside a vacuum chamber and using the three distinct energies of the α -particles of a ^{241}Am source at 5.486 MeV, 5.443 MeV, and 5.388 MeV for the energy calibrations.

To prove that the detector's energy range as based on the development is able to cope with heavy charged particles as encountered in the space radiation environment, calibrations and tests of the M-42 systems have been performed at the National Institute of

Radiological Sciences (NIRS) using the Heavy Ion Medical Accelerator (HIMAC) facility in Chiba, Japan. Irradiations were performed in the frame of the HIMAC Research Project 17H374 "Space Radiation Dosimetry—Energetic Particle Detection with Active and Passive Detector Systems for Space Missions." Figure 8 provides the setup of the M-42_C detector in the Physics Room at HIMAC showing the M-42_C detector with the batteries and the USB cable connected for online data readout. In front of the detector is a scintillation counter and in front of this is the beam exit with an ion beam with a diameter of around one cm.

The energy deposition spectra measured with the M-42_C system upon exposure to various ions, such as protons, helium, carbon, oxygen, and neon, are provided in Fig. 9. For better comparison purposes, only the main peaks of the relevant spectra are shown in a normalized way.

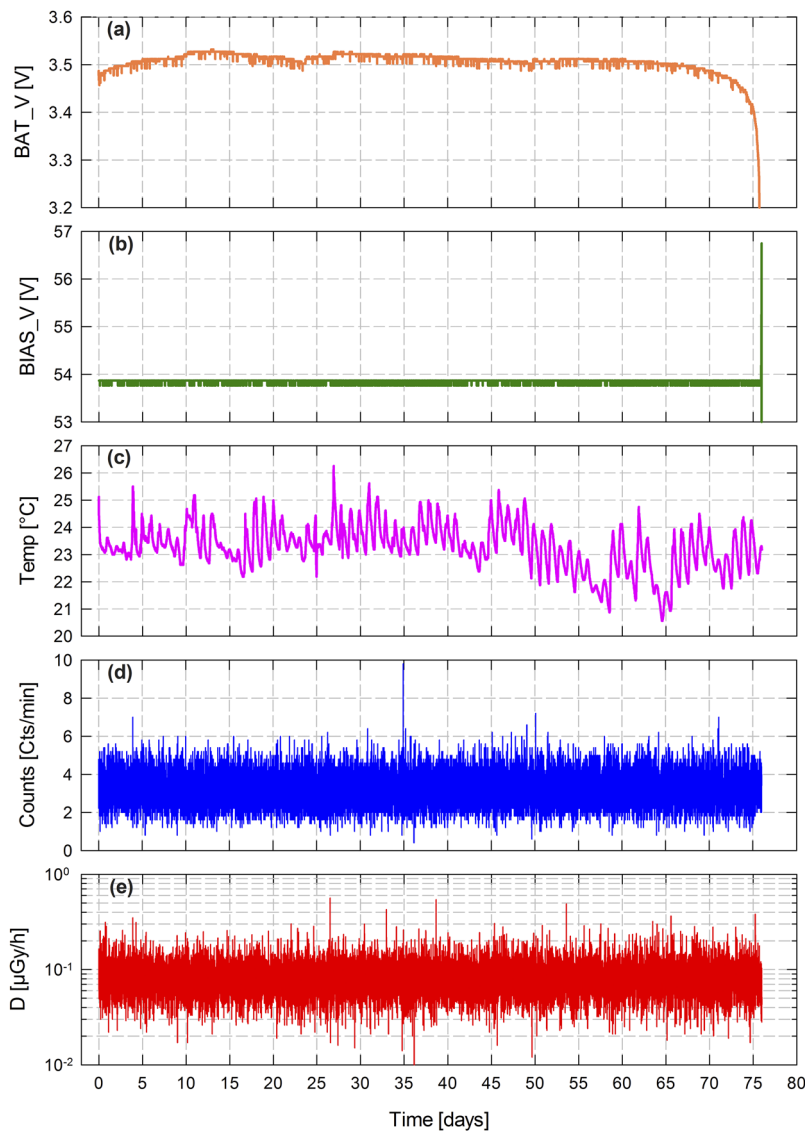


FIG. 11. Data from the long term battery test: (a) battery voltage (BAT_V), (b) bias high voltage of the diode (BIAS_V), (c) temperature sensor data, (d) count rate, and (e) absorbed dose rate in $\mu\text{Gy/h}$ in H_2O .

As a further example of the (by design) increased energy range of the M-42_D detector (see also Table I), Fig. 10 shows a comparison of counts measured with M-42_C and M-42_D after irradiation with 490 MeV/n silicon ions. While the M-42_C shows a peak in the overflow channel at 18 MeV energy depositions in Si, the M-42_D clearly resolves the peak of the applied ion beam and shows subsequently the overflow channel at 43 MeV energy depositions in the detector.

B. Battery test

The M-42 system was also developed to act as one of the detectors applied in the detector suit of the MARE experiment on-board the NASA Artemis I mission to the Moon. For this, the detector has to be able to record data and work without external power and data interface for a maximum mission duration of 42 days. In addition, the detector has to be able to bridge a time span of up to several weeks on the launch pad prior to launch during which no access to the detector is possible. This gives the necessity to have a battery-powered detector system with low power consumption without compromising the science output.

In the following data will be presented of a long term battery test of the M-42_C detector measuring in flight configuration equipped with two 2600 mAh primary batteries connected in parallel. The results of this long term test are presented in Figs. 11 and 12. The measurements lasted for 76.02 days and stopped when the battery voltage dropped below the 3.2 V necessary for the electronics to work. The relevant data are presented in Figs. 11(a)–11(c) showing the battery voltage (BAT_V), the bias voltage for the silicon diode (BIAS_V), as well as the data from the internal temperature sensor (Temp) (all H/K data of the system). In addition, the measured count rates are provided in Fig. 11(d) and the measured dose rates are given in Fig. 11(e). The count and dose rates have to be seen as the nominal background radiation encountered in the Biophysics lab at DLR, Cologne, Germany. The data show an average count rate of 3.2 ± 0.8 cts/min and an average absorbed dose rate of 85 ± 31 nGy/h, which leads to a daily absorbed dose of $2.05 \mu\text{Gy}$ in H_2O . Furthermore, the relevant energy

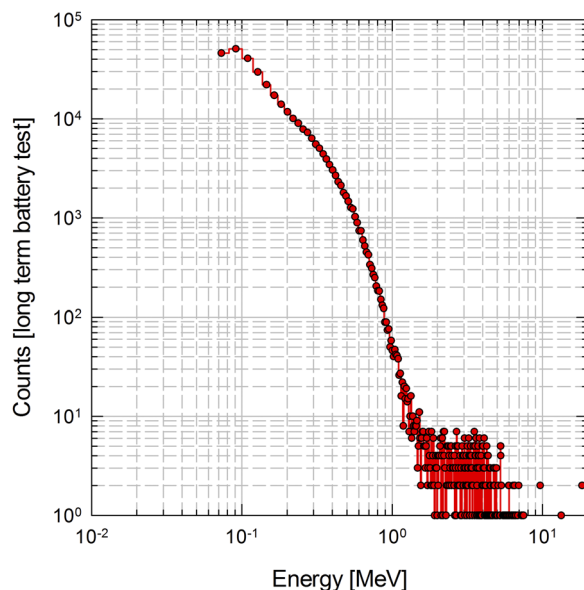


FIG. 12. Energy deposition spectrum for the 76.02 days of background measurement at DLR.

deposition spectrum for this long term measurement is provided in Fig. 12.

C. EMC test

A detector system used for applications in human space flight has to cope with relevant requirements for EMC (Electro-Magnetic Compatibility). Hereby, the focus for battery powered systems has to be mostly on the relevant radiated emissions of the system under study. Therefore, an EMC test was performed at the DLR Institute of Space Systems, Bremen, Germany. The test was performed according to MIL-STD-461F norm. Figure 13 shows the measured radiated emissions that are in the whole spectrum range below the specified limits.

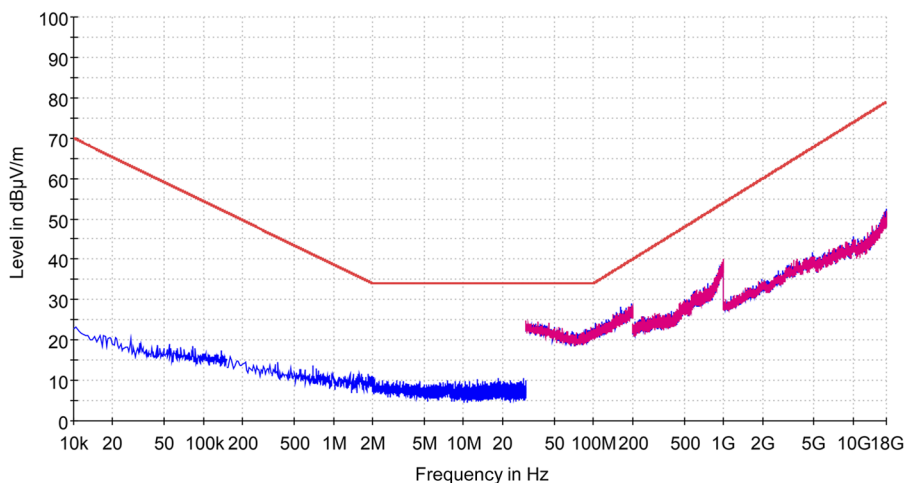


FIG. 13. EMC radiated emission test results of M-42_C. Blue, vertical antenna polarization; red, horizontal antenna polarization; and orange, test limits.

IV. M-42 RESULTS OF IN-FLIGHT EXPERIMENTS

In the following, we are going to provide data from measurements in complex radiation fields accomplished with various versions of the M-42 system. In Subsection IV A, we present data from measurements on airplanes, and in Subsection IV B, we present data from two DLR MAPHEUS flight campaigns, namely, MAPHEUS-7 in February 2018 and MAPHEUS-8 in June 2019. For both examples, also comparisons with GEANT4 Monte Carlo calculations are provided.

A. Airplane flights

In the frame of the last few years, data have been collected for long haul flights from Europe to Japan and the USA applying various versions of the M-42 system. In the following, we present some exemplary data for a flight to and from Japan (Düsseldorf, Germany to Narita, Japan). For these flights, the integration time of the M-42 detectors (M-42_C and M-42_D) was set to 5 min. In addition to the measurements, the absorbed dose values in Si were also calculated applying the DLR Professional Aviation Dose

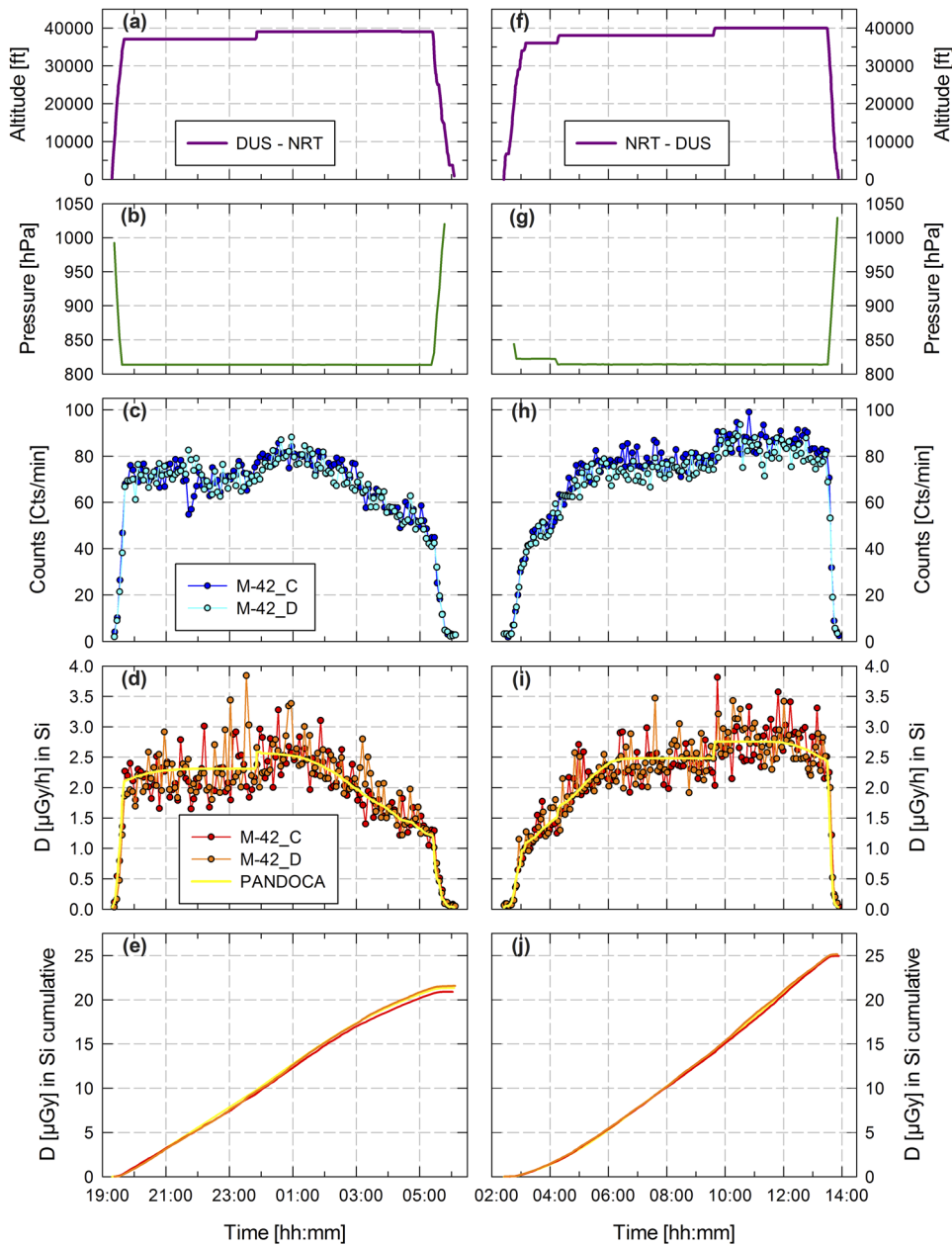


FIG. 14. (a) and (f) Flight level for the flight from Düsseldorf (DUS), Germany to Tokyo Narita (NRT), Japan, and from NRT to DUS; (b) and (g) measured cabin pressure for the flights; (c) and (h) count rates; (d) and (i) absorbed dose rates in Si as well as the absorbed dose rate in Si calculated with the DLR PANDOCA model; and (e) and (j) cumulative dose for the data given in (d) and (i).

TABLE III. Results of the measurements of the total flight absorbed dose in Si compared with the DLR PANDOCA calculations.

	Absorbed dose (μGy) in Si		
	M-42_C	M-42_D	PANDOCA
DUS-NRT	20.9 ± 0.4	21.6 ± 0.4	21.3 ± 1.1
NRT-DUS	25.0 ± 0.5	25.1 ± 0.5	25.0 ± 1.2

Calculator (PANDOCA) program.²¹ The relevant data for the flight are presented in Fig. 14 and in Table III.

Figure 14 shows in (a) and (f) the relevant flight levels [altitude (ft)] and in (b) and (g) the relevant measured pressure with the internal pressure sensor of the M-42_D detector [pressure (hPa)]. Furthermore, Figs. 14(c) and 14(h) provide the count rates measured with the M-42_C and the M-42_D detector, (d) and (i) show the dose rate (in Si), and (e) and (j) provide the cumulative absorbed dose in Si for the respective flights. In addition, Figs. 14(d)–14(j) also compare the results for the dose rate in Si calculated with the DLR PANDOCA model²¹ to the measurements on the respective flights. The dose rate in Si is calculated in PANDOCA for a 0.3 mm silicon slab using the secondary particle fluence from galactic cosmic radiation (GCR) at a given altitude and position. The primary GCR spectra are derived from the model described in Ref. 22 using the average daily neutron monitor count rates by the Oulu station (<http://cosmicrays oulu.fi/>). The data for the two flights in terms of accumulated flight dose are also presented in Table III. On the flight from DUS to NRT, a total calculated dose in silicon of $21.3 \pm 1.1 \mu\text{Gy}$ and a peak dose rate of $2.6 \mu\text{Gy/h}$ (at 39 kft) were reached. In comparison, the total dose for the flight measured with the M-42_C was $20.9 \pm 0.4 \mu\text{Gy}$ and with the M-42_D $21.6 \pm 0.4 \mu\text{Gy}$. On the return flight, the calculated total dose was $25.0 \pm 1.2 \mu\text{Gy}$ and the peak dose rate was $2.8 \mu\text{Gy/h}$ (at 40 kft). M-42_C measured a total flight dose of $25.0 \pm 0.5 \mu\text{Gy}$, while M-42_D provided a total dose of $25.1 \pm 0.5 \mu\text{Gy}$.

Data comparison proves that the results are in very close proximity to the GEANT4 Monte Carlo calculations for the two respective flights.

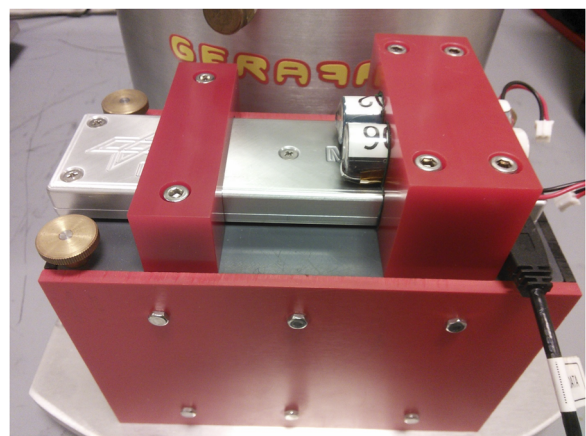
B. The MAPHEUS campaigns

The MAPHEUS (Materialphysikalische Experimente unter Schwerelosigkeit—material physics experiments under weightlessness) high-altitude research program prepared and carried out by DLR's MORABA (Mobile Raketenbasis—mobile rocket base) department gives scientists independent and regular access to experiments in weightlessness. The two stage MAPHEUS-7 research rocket was launched by DLR from the Esrange Space Center rocket launch site on February 17, 2018 at 8 a.m., reaching an altitude of 247.6 km and more than 6 min of weightlessness. The mission objectives were to successfully carry out the six μ -gravity experiments on board and to qualify the newly developed S31-Improved Malemute launcher system, which placed increased demands on the payload's resistance to accelerations. The high-altitude research rocket carried a payload of 365 kg on a sub-orbital trajectory. On June 13, 2019 at 4:21 a.m. the ATEK mission

(Propulsion Technologies and Components for Launcher Systems) of DLR transported health monitoring systems for critical launcher components, a hybrid housing structure and the MAPHEUS-8 payload consisting of various biological and materials science experiments to an altitude of around 240 km.

The two MAPHEUS campaigns offered the perfect opportunity to test various functions of the M-42 detector system. The first test was the functionality of the built-in accelerometer of the M-42 detector. The system is in SLEEP MODE (low power consumption) upon installation in the rocket and will only be switched on after the accelerometer detects acceleration for a certain amount of time. With this, the system is switched from SLEEP to MEAS MODE. The second test was the measurement of the count and dose rate during the MAPHEUS-7 (M7) and -8 (M8) campaigns. For the measurements of count and dose rate, the internal timestamp was set for a 5 s time interval. This was chosen to (a) clearly define the changes of acceleration and μ -gravity and (b) to map the around 6 min of μ -gravity with reasonable statistics. For the M7 and M8 flights, the applied M-42_C system was mounted in a piggyback configuration to the CellFix payload of the Gravitational Biology group experiment of the Institute of Aerospace Medicine (Fig. 15).

Figure 16 shows the first 20 min of the measurements of the count- [Fig. 16(a)] and dose rates [Fig. 16(b)] for both campaigns in comparison. The M-42_C system was in SLEEP MODE after the installation in the rocket. Upon launch, the accelerometer started the measurement and puts the system into MEAS MODE. As a consequence, the internal clock is set to zero and starts counting. After around 1 min, the rocket reached 100 km in altitude and the μ -gravity phase started. Within the first minute of the measurements, the count and dose rates were high due to the fact that the vibration of the rocket induces microphonic effects in the diode. Upon reaching the μ -gravity phase, this microphonic effects stopped and the undisturbed radiation data for the next 6 min were recorded. Shortly, after minute seven of the mission the parachutes were deployed, inducing again microphonic effects in the diode and shortly afterward the rockets landed on the ground. Interestingly,

**FIG. 15.** M-42_C radiation detector with two primary batteries mounted in a piggyback configuration to the CellFix payload provided by the Gravitational Biology Group of the Institute of Aerospace Medicine for the MAPHEUS campaigns.

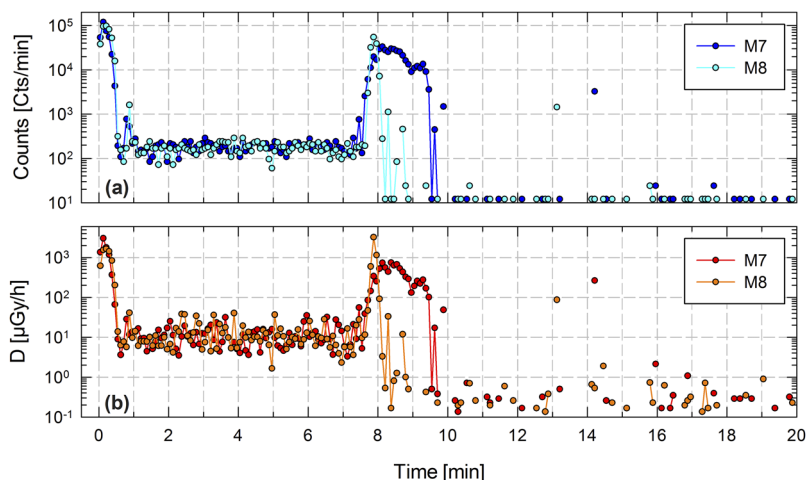


FIG. 16. Comparison of M7 and M8 for a time period of 20 minutes: (a) count rate and (b) absorbed dose rate in $\mu\text{Gy/h}$ in H_2O .

MAPHEUS-7 landed approximately ten minutes after launch, while MAPHEUS-8 landed already 8 min after launch. After landing the M-42 system recorded the nominal background radiation dose on ground with short exceptions at around minutes 13 and 14 where

the rocket turned over and increased again the count- and dose rate by the induction of microphonic effects.

Figure 17 provides for both missions the count- [Figs. 17(a) and 17(d)] and dose rate [Figs. 17(b) and 17(e)] for the 6 min of

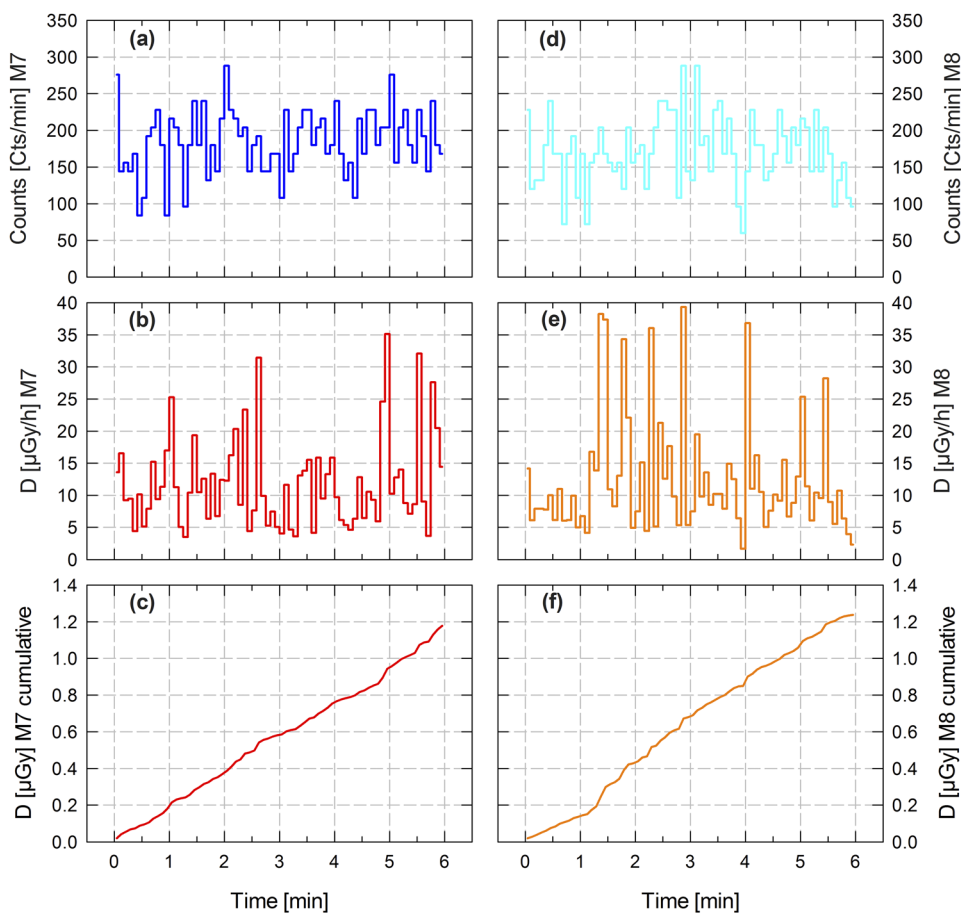


FIG. 17. Comparison of MAPHEUS-7 and -8 for the 6 min of μ -gravity: (a) and (d) count rates for M7 and M8, (b) and (e) absorbed dose rates in H_2O for M7 and M8, and (c) and (f) cumulative dose over the 6 min of μ -gravity.

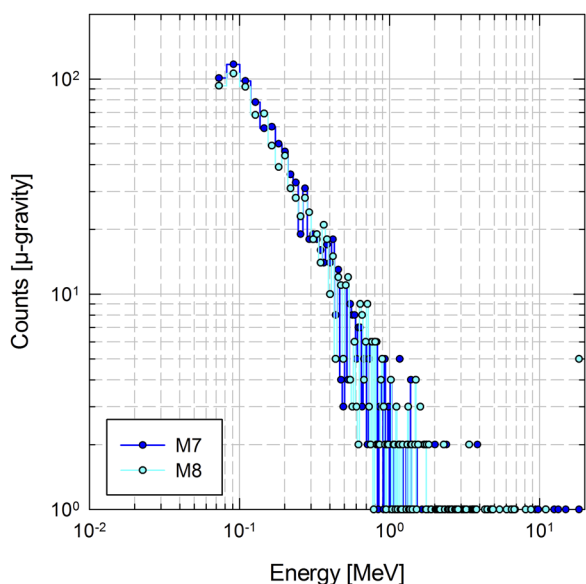


FIG. 18. Energy deposition spectra for the M-42 instruments for the M7 and the M8 flight for the 6 min of μ -gravity duration.

μ -gravity. The average count rates for M7 are 184 ± 44 cts/min and for M8 170 ± 48 cts/min. Absorbed dose rates are on average $11.8 \mu\text{Gy/h}$ (in H_2O) measured for M7 and $12.4 \mu\text{Gy/h}$ (in H_2O) for M8. This is in very good agreement with data measured currently with the RAMIS detector on the DLR Eu:CROPIS mission. The total average dose for the MAPHEUS-7 and -8 μ -gravity phase (6 min) accounts to $1.18 \pm 0.11 \mu\text{Gy}$ and $1.24 \pm 0.11 \mu\text{Gy}$, respectively [Figs. 17(c) and 17(f)], which equals around half a day of background radiation dose on Earth. The relevant energy deposition spectra for both missions are provided in Fig. 18 for the 6 min of the μ -gravity phase. As can be seen, both spectra are almost identical for the two missions.

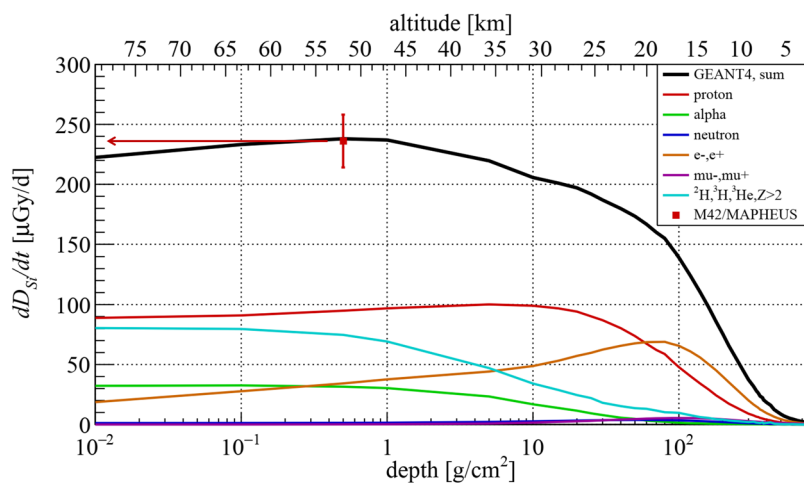


FIG. 19. Calculated dose rates in silicon from GCR vs atmospheric depth (altitude) compared to measurements performed during the M8 campaign. The symbol for the measurement was placed at 0.5 g/cm^2 to consider the additional shielding provided by the detector housing; the actual measurement was performed at much higher altitudes (up to 250 km as illustrated by the arrow).

The experimental result for the dose rate in silicon measured during the MAPHEUS-8 campaign is further compared to results of a numerical simulation in Fig. 19. For the simulation, the PLANETOCOSMICS (<http://cosray.unibe.ch/~laurent/planetocosmics/>) toolkit for GEANT4 has been used similarly to simulations performed for the Martian atmosphere,^{23,24} i.e., using the identical primary GCR model²¹ but adapted for the date of the actual flight (June 13, 2019), the identical physics list in GEANT4, the same secondary particles, but of course changing the atmospheric conditions using the description of Earth's atmosphere (NRLMSISE-00 model²⁵), as implemented in PLANETOCOSMICS. The magnetic shielding at the location is negligible and the calculated cutoff rigidity for the launch site of the rocket (68°N , 21°E) is $R_C \approx 0.3 \text{ GV}$, which corresponds in the case of protons to a kinetic energy of 47 MeV and in the case of alpha particles to a kinetic energy of 12.0 MeV/n. The number of primary particles below this threshold constitute significantly less than 1% of the total dose.

Figure 19 illustrates the calculated dose rate in silicon as a function of atmospheric depth and compares the results with the M-42 measurements during the MAPHEUS-8 campaign. The dose rate in silicon measured by the M-42_C instrument during the campaign was $241 \pm 22 \mu\text{Gy/d}$. It should be noted that the dose rates in the numerical simulation are calculated for a single slab of silicon but the detector itself is surrounded by the detector housing and the payload compartment which means that the detector never is at zero shielding. As a consequence, the measured value should be rather compared to the calculated value at approximately 0.5 g/cm^2 (2 mm Al housing), although the measurement was performed effectively outside the atmosphere.

With increasing altitudes, the calculated dose rate increases up to approximately 50 km reaching a maximum value of $238 \mu\text{Gy/d}$ and slowly decreases at higher altitudes. The increase in dose rate is especially pronounced at altitudes below 25 km. In addition to the total dose rate, Fig. 19 also shows the individual contributions of different particle types with protons, alphas, and heavier nuclei being the dominant component at high altitudes. At lower altitudes, electrons (e^-) and positrons (e^+) become increasingly important and even exceed the contribution of protons at altitudes below approximately 20 km.

V. SUMMARY

The Biophysics Group at DLR has developed and is further developing a system of small, easy to use, and easy to expand radiation detectors for relevant research topics in the frame of radiation measurements, radiation protection, and radiation dosimetry. Currently, this family has three members, namely, the M-42_C, the M-42_S, and the M-42_D system. It has been shown that the systems are capable of working as dosimetric instruments, relevant calibrations have been performed at HIMAC, NIRS, Japan, and the system has been proven to work in space during the two MAPHEUS missions. Furthermore, results of the measurements have been compared to relevant GEANT4 Monte Carlo calculations and showed good agreement. DLR will further work on upgrades for the M-42 detector family.

ACKNOWLEDGMENTS

The authors would like to thank the Sodankyla Geophysical Observatory and the website teams (<http://cosmicrays oulu.fi>) for providing the Oulu neutron monitor data. The authors would like to thank the colleagues from the DLR Institute of Space Systems in Bremen for performing the EMC test and the colleagues from the DLR MORABA group and the ESRANGE colleagues for working on a flawless MAPHEUS-7 and -8 campaigns. We would also like to thank all colleagues at NIRS Chiba Japan, especially Satoshi Kodaira and Hisashi Kitamura and the staff members of the HIMAC team for the support during the HIMAC calibration campaigns. Work performed for the development of the M-42 detector was supported by DLR under Grant FuW 2475019.

REFERENCES

- ¹C. S. Warren and W. L. Gill. *Radiation Dosimetry Aboard the Spacecraft of the Eight Mercury-Atlas Mission (MA-8)*. NASA TN D-1862 (U.S. Govt. Printing Office, Washington, DC, 1964).
- ²T. Berger, B. Przybyla, D. Matthiä, G. Reitz, S. Burmeister *et al.*, “DOSIS & DOSIS 3D: Long term dose monitoring onboard the columbus laboratory of the International Space Station (ISS),” *J. Space Weather Space Clim.* **6**, A39 (2016).
- ³L. Narici, T. Berger, D. Matthiä, and G. Reitz, “Radiation measurements performed with active detectors relevant for human space exploration,” *Front. Oncol.* **5**, 273 (2015).
- ⁴T. P. Dachev, F. Spurny, G. Reitz, B. T. Tomov, P. G. Dimitrov, and Y. N. Matviichuk, “Simultaneous investigation of galactic cosmic rays on aircrafts and on International Space Station,” *Adv. Space Res.* **36**, 1665–1670 (2005).
- ⁵T. Dachev, W. Atwell, E. Semones, B. Tomov, and B. Reddell, “Observations of the SAA radiation distribution by Liulin-E094 instrument on ISS,” *Adv. Space Res.* **37**, 1672–1677 (2006).
- ⁶T. P. Dachev, B. T. Tomov, Y. N. Matviichuk, P. S. Dimitrov, S. V. Vadawale, J. N. Goswami, G. De Angelis, and V. Girish, “An overview of RADOM results for earth and moon radiation environment on Chandrayaan-1 satellite,” *Adv. Space Res.* **48**, 779–791 (2011).
- ⁷A. E. Lishnevskii, M. I. Panasyuk, V. V. Benghin, V. M. Petrov, A. N. Volkov, and O. Y. Nechaev, “Variations of radiation environment onboard the ISS in the year 2008,” *Cosmic Res.* **48**(3), 206–210 (2010).
- ⁸A. Lishnevskii, M. I. Panasyuk, V. V. Benghin, V. M. Petrov, A. N. Volkov, and O. Y. Nechaev, “Variations of radiation environment on the International Space Station in 2005–2009,” *Cosmic Res.* **50**(4), 319–323 (2012).
- ⁹T. Berger, S. Burmeister, D. Matthiä, B. Przybyla, G. Reitz *et al.*, “DOSIS & DOSIS 3D: Radiation measurements with the DOSTEL instruments onboard the Columbus Laboratory of the ISS in the years 2009–2016,” *J. Space Weather Space Clim.* **7**, A08 (2017).
- ¹⁰B. Zäbori, A. Hirn, S. Deme, I. Apáthy, C. Antal, T. Pázmándi, and P. Szántó, “Space dosimetry measurements in the stratosphere using different active and passive dosimetry systems,” *Radiat. Prot. Dosim.* **171**(4), 453–462 (2016).
- ¹¹L. Narici, T. Berger, S. Burmeister, L. Di Fino, A. Rizzo, D. Matthiä, and G. Reitz, “Exploiting different active silicon detectors in the International Space Station: ALTEA and DOSTEL Galactic Cosmic Radiation (GCR) measurements,” *J. Space Weather Space Clim.* **7**, A18 (2017).
- ¹²D. Hassler, C. Zeitlin, R. Wimmer-Schweingruber, S. Böttcher, C. Martin *et al.*, “The Radiation Assessment Detector (RAD) investigation,” *Space Sci. Rev.* **170**(1–4), 503–558 (2012).
- ¹³D. M. Hassler, C. Zeitlin, R. F. Wimmer-Schweingruber, B. Ehresmann *et al.*, “Mars surface radiation environment measured with the mars science laboratory’s curiosity rover,” *Science* **343**(6169), 1244797 (2014).
- ¹⁴C. Zeitlin, D. Hassler, F. Cucinotta, B. Ehresmann, R. Wimmer-Schweingruber *et al.*, “Measurements of energetic particle radiation in transit to mars on the mars science laboratory,” *Science* **340**(6136), 1080–1084 (2013).
- ¹⁵T. Berger, D. Matthiä, S. Burmeister, R. Rios, K. Lee *et al.*, “The Solar Particle Event on 10 September 2017 as observed on-board the International Space Station (ISS),” *Space Weather* **16**, 1173–1189 (2018).
- ¹⁶R. Gaza, M. Kroupa, R. Rios, N. Stoffle, E. R. Benton, and E. Semones, “Comparison of novel active semiconductor pixel detector with passive radiation detectors during the NASA Orion Exploration Flight Test 1 (EFT-1),” *Radiat. Meas.* **106**, 290–297 (2017).
- ¹⁷J. Hauslage, S. M. Strauch, O. Eßmann, F. W. M. Haag, P. Richter *et al.*, “Eu:CROPIS—Euglena gracilis: Combined regenerative organic-food production in space”—A space experiment testing biological life support systems under lunar and martian gravity,” *Microgravity Sci. Technol.* **30**(6), 933–942 (2018).
- ¹⁸G. Reitz, T. Berger, P. Bilski, R. Facius, M. Hajek *et al.*, “Astronaut’s organ doses inferred from measurements in a human phantom outside the International Space Station,” *Radiat. Res.* **171**(2), 225–235 (2009).
- ¹⁹C. La Tessa, T. Berger, R. Kaderka, D. Schardt, S. Burmeister, J. Labrenz, G. Reitz, and M. Durante, “Characterization of the secondary neutrons field produced during treatment of an anthropomorphic phantom with x-rays, protons and carbon ions,” *Phys. Med. Biol.* **59**, 2111–2125 (2014).
- ²⁰J. Labrenz, S. Burmeister, T. Berger, B. Heber, and G. Reitz, “Matroshka DOSTEL measurements onboard the International Space Station (ISS),” *J. Space Weather Space Clim.* **5**, A38 (2015).
- ²¹D. Matthiä, M. M. Meier, and G. Reitz, “Numerical calculation of the radiation exposure from galactic cosmic rays at aviation altitudes with the PANDOCA core model,” *Space Weather* **12**(3), 161–171 (2014).
- ²²D. Matthiä, T. Berger, A. I. Mrigakshi, and G. Reitz, “A ready-to-use galactic cosmic ray model,” *Adv. Space Res.* **51**, 329–338 (2013).
- ²³D. Matthiä and T. Berger, “The radiation environment on the surface of Mars—Numerical calculations of the galactic component with GEANT4/PLANETOCOSMICS,” *Life Sci. Space Res.* **14**, 57–63 (2017).
- ²⁴D. Matthiä *et al.*, “The radiation environment on the surface of Mars—Summary of model calculations and comparison to RAD data,” *Life Sci. Space Res.* **14**, 18–28 (2017).
- ²⁵J. M. Picone, A. E. Hedin, D. P. Drob, and A. C. Aikin, “NRLMSISE-00 empirical model of the atmosphere: Statistical comparisons and scientific issues,” *Journal of Geophysical Research: Space Physics* **107**(A12), SIA 15–1–SIA 15–16 (2002).